Repository Istituzionale dei Prodotti della Ricerca del Politecnico di Bari

Rough contact of sliding viscoelastic layers: Numerical calculations and theoretical predictions

This is a post print of the following article

Original Citation:
Rough contact of sliding viscoelastic layers: Numerical calculations and theoretical predictions / Menga, N.; Afferrante, L.; Demelio, G. P.; Carbone, G.. - In: TRIBOLOGY INTERNATIONAL. - ISSN 0301-679X. - ELETTRONICO. - 122:(2018), pp. 67-75. [10.1016/j.triboint.2018.02.012]

Availability:
This version is available at http://hdl.handle.net/11589/122877 since: 2022-05-31

Published version
DOI:10.1016/j.triboint.2018.02.012

Publisher:

Terms of use:

(Article begins on next page)

02 May 2026

Accepted Manuscript

Rough contact of sliding viscoelastic layers: Numerical calculations and theoretical predictions

N. Menga, L. Afferrante, G.P. Demelio, G. Carbone

PII: S0301-679X(18)30093-8

DOI: 10.1016/j.triboint.2018.02.012

Reference: JTRI 5111

To appear in: *Tribology International*

Received Date: 20 December 2017

Revised Date: 8 February 2018

Accepted Date: 10 February 2018

Please cite this article as: Menga N, Afferrante L, Demelio GP, Carbone G, Rough contact of sliding viscoelastic layers: Numerical calculations and theoretical predictions, *Tribology International* (2018), doi: 10.1016/j.triboint.2018.02.012.

This is a PDF file of an unedited manuscript that has been accepted for publication. As a service to our customers we are providing this early version of the manuscript. The manuscript will undergo copyediting, typesetting, and review of the resulting proof before it is published in its final form. Please note that during the production process errors may be discovered which could affect the content, and all legal disclaimers that apply to the journal pertain.

ACCEPTED MANUSCRIPT

Rough contact of sliding viscoelastic layers: numerical calculations and theoretical predictions

N. Menga,[1,*] L. Afferrante,[1] G.P. Demelio,[1] and G. Carbone[1,2,3]

[1]*Department of Mechanics, Mathematics and Management, Politecnico of Bari, V.le Japigia, 182, 70126, Bari, Italy*
[2]*CNR - Institute for Photonics and Nanotechnologies U.O.S. Bari, Physics Department "M. Merlin", via Amendola 173, 70126 Bari, Italy*
[3]*Imperial College London, Department of Mechanical Engineering, Exhibition Road, London SW7 2AZ*

Abstract

We study the sliding contact of viscoelastic layers on rigid rough profiles, with two different contact configurations: constrained on the upper boundary, and uniformly loaded on the top.

Results show that layer thickness and boundary conditions affect both the average contact quantities and the viscoelastic friction. Interestingly, the latter is strongly influenced by the specific controlled parameter. Under displacement controlled conditions, large differences are observed in the frictional behavior of the two contact configuration. Conversely, in load control, the friction coefficient is almost independent of the specific boundary condition.

Finally, a comparison with a 1D version of the Persson's theory is proposed, finding a good agreement in terms of dependence of contact area and friction coefficient on the sliding velocity.

Keywords: Rough contact mechanics, viscoelasticity, friction, thin layers

ACCEPTED MANUSCRIPT

*Electronic address: [Correspondingauthor.]Email:nicola.menga@poliba.it,phonenumber: +390805962746

I. INTRODUCTION

Polymeric rubber-like materials are nowadays spreading well beyond the classical applications (e.g., tyres, seals, dampers) even towards micro scales devices, protective films, thin gloves and suits, bio-inspired layers mimicking skin.

Several tribological phenomena, like friction and adhesion [1–3], as well as wear [4–7], percolation [8, 9], thermal [10, 11] and electrical [12] conductance between surfaces, etc..., can be understood and explained only considering the multiscale nature of the rough surfaces. Several studies address the problem of predicting the contact behavior of semi-infinite solids. Specifically, the theoretical approaches available in the literature can be grouped in two categories: (i) the multiasperity contact models based on the original idea of the pioneering works of Archard [13] and Greenwood&Williamson (GW) [14] (the ultimate version given in Bush, Gibson and Thomas (BGT) [15] and the recent development proposed in Ref. [16] are part of this category), and (ii) the theoretical approach by Persson [17] (included some recent works improving the theory [18–20]). Furthermore, there are also many numerical studies [21–32], specific molecular dynamics (MD) simulations [33], and experimental investigations [34–39] devoted to this problem. However, less attention has been paid to the case of contact involving bodies of finite thickness, despite an accurate representation of contact stresses and deflections between sliding coated bodies is of fundamental importance in tribological applications. Coatings are widely used in friction components to reduce friction and to increase wear resistance, life and durability.

One of the first attempt to investigate the contact behavior of viscoelastic layered systems has been made in [40], where deformation, friction dissipation and contact stresses are calculated under the action of a moving load. An analytical solution is instead proposed in Ref. [41] for a single layered viscoelastic material bonded to a rigid substrate and in frictionless contact with a rigid smooth indenter. Furthermore, in Ref. [42], it has been shown that contact pressure and internal stress distributions are significantly affected by viscoelastic properties and sliding velocity. In particular, the presence of a viscoelastic layer on a rigid or elastic foundation causes the pressure to become non-symmetrical. More recently, Persson has extended his contact mechanics model to layered materials [43], and has investigated the contact behavior of a rigidly constrained viscoelastic layer [44].

The finite size of contacting bodies can affect significantly the contact behavior when the contact spots reach a size comparable with the body thickness (see, for example, Ref. [45]). Moreover, the contact solution is strongly affected by the boundary conditions as shown in Ref. [2, 46, 47], where the periodic elastic and viscoelastic sliding contact between finite-sized bodies is investigated. Indeed, depending on whether a uniform pressure or a rigid constraint is applied on the upper boundary of the layer, the contact stiffness is found increasing or decreasing with the thickness. Moreover, thickness plays a key role in determining the amount of energy dissipated in the bulk of material, whereas boundary conditions mainly affect the fundamental exciting frequency at which the largest dissipation occurs.

These works focus on smooth or one scale rough contacts; however, since all engineering surfaces are rough to some degree, accounting for the effects of surface topography is critical to model the contact. The importance of such a topic is also demonstrated by the recently published contact-mechanics challenge where several scientists from across the world set up a comparison between the most advanced theories to precisely address the rough contact mechanics problem (see Ref.[48] and the bibliography therein included). A first consequence

of the multiscale nature of roughness is the presence of a broader spectrum of frequencies exciting the material. This is taken into account in Ref. [37], where the theory of contact mechanics and rubber friction developed by Persson is extended to the case of surfaces with anisotropic roughness, and in Ref. [49], where a boundary element methodology is developed to calculate frictional losses in layered systems. In the first work, it is shown that the friction coefficient may depend significantly on the sliding direction, differently from the contact area which depends weakly on it. In the latter, it is instead point out that significantly changes in viscoelastic dissipation can occur owing to the finite thickness of the surface layer. Interesting results have been found also with respect to transient sliding condition in Ref. [50] (with peculiar attention to the case of start from rest), and in Refs [51, 52] where, in the framework of the Persson's contact mechanics theory [18], the effect of roughness on viscoelastic contact area and friction is investigated. Adhesive rough contact mechanics has been investigated in Ref. [53], where the effect of the roughness scale on the effective energy of adhesion and pull-off tractions is explored.

In the present paper, we extend the analysis given in Ref. [46] to the case of contact between randomly rough profiles. Specifically, calculations are performed on self-affine profiles and viscoelastic material with one relaxation time. The bulk friction, due to the hysteretic behavior of the viscoelastic material, is also calculated under both load and displacement controlled conditions, and a full comparison with a 1D version of the Persson's theory [18] is proposed.

II. THE PROBLEM FORMULATION

Fig. 1 shows the problem under investigation: a linear viscoelastic layer of finite thickness sliding at constant velocity V on a rigid periodic rough profile with fundamental wavelength λ. Two contact configurations are considered: (a) a layer rigidly confined on the upper boundary (Fig. 1a), and (b) a free layer uniformly loaded on the top (Fig. 1b). The contact penetration is defined as $\Delta = u_{tot} - u_m$ (see Fig. 1c), where u_m and u_{tot} are the mean displacement of the viscoelastic body and the displacement of the rigid indenter, respectively. Moreover, we neglect interfacial tangential interactions (e.g. Coulomb's friction) and assume small deformations.

According to Ref. [27, 46, 54], the local displacement field (measured from the deformed mean plane) of the viscoelastic body can be written as

$$u(x) = -\int_{\Omega} G_V(x-s)\, p(s)\, ds \tag{1}$$

where Ω is the contact domain, and $G_V(x)$ is the viscoelastic Green's function for steady sliding contacts, which parametrically depends on the sliding speed V,

$$G_V(x) = J\left(0^+\right)\Gamma(x) + \int_{0^+}^{+\infty} \Gamma(x+Vt)\,\dot{J}(t)\, dt \tag{2}$$

being $\Gamma(x)$ the elastic-like Green's function for the contact problem at hand, and $J(t)$ the viscoelastic creep function. For a linear viscoelastic material with one relaxation time τ, $J(t)$ takes the form

$$J(t) = H(t)\left[\frac{1}{E_0} - \frac{1}{E_1}\exp\left(-t/\tau\right)\right] \tag{3}$$

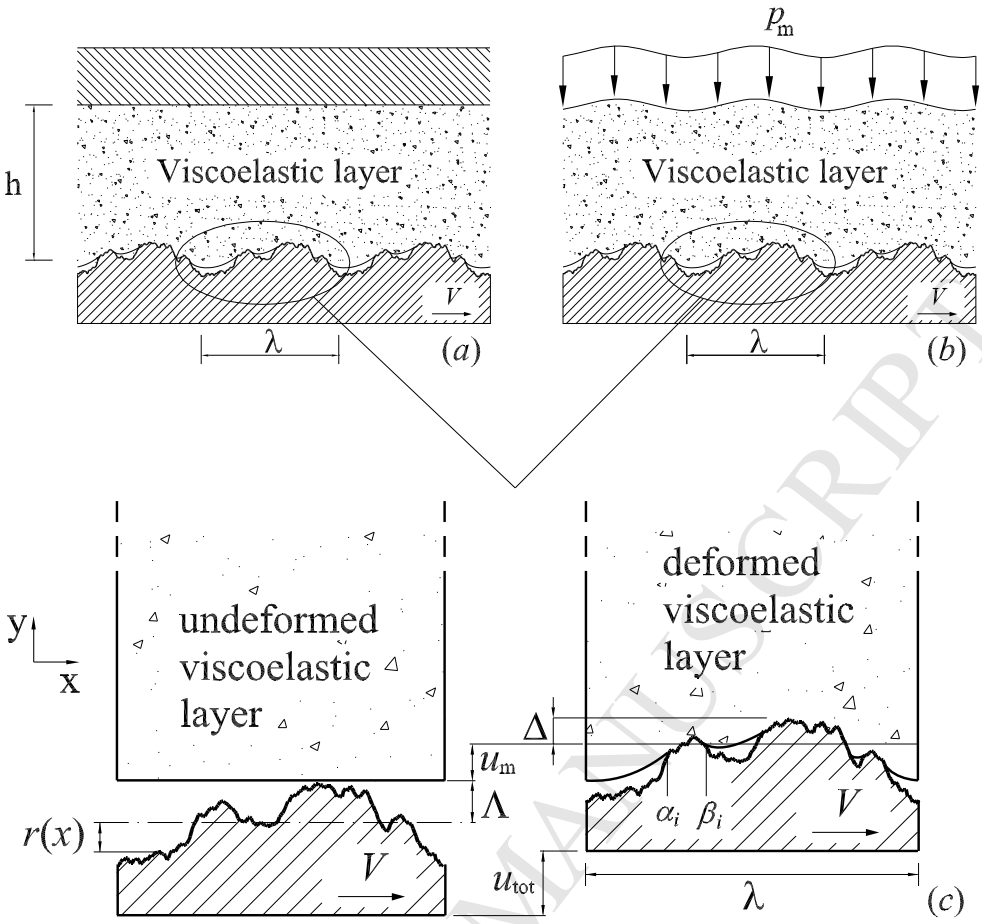

FIG. 1: The two contact configurations under investigation: a viscoelastic layer of thickness h rigidly contrained (a), and uniformly loaded (b) on the upper boundary. A magnification of the base periodic cell si shown in (c).

where $H(t)$ is the Heavyside step function, and $1/E_1 = 1/E_0 - 1/E_\infty$, being E_0 and E_∞ respectively the zero-frequency and high frequency elastic moduli of the material.

Finally, the expression of $\Gamma(x)$ for the contact configurations shown in Fig. 1 can be recovered from Ref. [45, 55]

$$\Gamma(x) = \frac{2(1-\nu^2)}{\pi}\left(\log\left[2\left|\sin\left(\frac{q_0 x}{2}\right)\right|\right] + \sum_{m=1}^{\infty} A_m(q_0 h)\frac{\cos(m q_0 x)}{m}\right) \tag{4}$$

where $q_0 = 2\pi/\lambda$, and

$$A_m(q_0 h) = \frac{2mq_0 h - (3-4\nu)\sinh(2mq_0 h)}{5 + 2(mq_0 h)^2 - 4\nu(3-2\nu) + (3-4\nu)\cosh(2mq_0 h)} + 1 \tag{5}$$

for the confined layer (Fig. 1a), and

$$A_m(q_0 h) = \frac{2mq_0 h + \sinh(2hmq_0)}{1 + 2(mq_0 h)^2 - \cosh(2mq_0 h)} + 1 \tag{6}$$

for the free layer (Fig. 1b).

For the displacement u_{m} of the mean plane we have

$$u_{\mathrm{m}} = \frac{1+\nu}{1-\nu}\frac{1-2\nu}{E_0}p_{\mathrm{m}}h \tag{7}$$

being $p_{\mathrm{m}} = \lambda^{-1}\int_{\Omega} p\left(x\right)dx$ the mean contact pressure.

Within the contact domain Ω, the elastic displacement is $u\left(x\right) = \Delta + r\left(x\right) - \Lambda$, where $r\left(x\right)$ is the local profile height and Λ is the local peak (see Fig. 1c). Therefore, substituting in Eq. (1), we can write

$$\Delta + r\left(x\right) - \Lambda = -\int_{\Omega} G_V\left(x-s\right)p\left(s\right)ds \qquad x \in \Omega \tag{8}$$

which is a Fredholm integral equation on the first kind for the unknown contact pressure distribution $p\left(x\right)$.

The above equation is solved by following the solution scheme firstly addressed in Ref. [45]. Hence, once known $G_V\left(x\right)$ for any given value of Δ and V, eq. (8) allows to numerically calculate $p\left(x\right)$ as a function of the unknown coordinates α_i and β_i of the i-th contact area, with $\alpha_i < \beta_i$ (see Fig. 1c). In fact, if N_c is the number of contact spots $[\alpha_i, \beta_i]$, the contact domain is $\Omega = \cup_{i=1}^{N_c}\left[\alpha_i, \beta_i\right]$.

Therefore, to completely define the contact problem, additional conditions are needed to determine the coordinates α_i and β_i. Such conditions, according to Ref. [46], are obtained by considering that, in the adhesiveless case, the mode I stress intensity factors at the edges of each contact area must vanish (Ref. [56])

$$K_{I,\alpha_i} = -\lim_{x\to\alpha_i^+}\sqrt{2\pi\left(x-\alpha_i\right)}p\left(x\right) = 0 \tag{9}$$

$$K_{I,\beta_i} = -\lim_{x\to\beta_i^-}\sqrt{2\pi\left(\beta_i-x\right)}p\left(x\right) = 0 \tag{10}$$

III. RESULTS FOR SELF-AFFINE RANDOMLY ROUGH PROFILES

Calculations are performed on a linear viscoelastic material with $E_\infty = 3E_0$ and Poisson's ratio $\nu = 0.5$ (i.e. incompressible material). Moreover, self-affine profiles are numerically generated as reported in appendix A with a Power Spectral Density (PSD) $C\left(q\right) = \left(2\pi\right)^{-1}\int\left\langle r\left(0\right)r\left(x\right)\right\rangle e^{-iqx}$given by

$$\begin{aligned} C\left(q\right) &= C_0\left(\frac{|q|}{q_0}\right)^{-(2H+1)} \qquad ; \qquad q \in [q_0, q_1] \\ C\left(q\right) &= 0; \qquad q > q_1 \end{aligned} \tag{11}$$

where $q_1 = Nq_0$ (being N the number of roughness scales) and H is the Hurst exponent, which is related to the fractal dimension $D_f = 2 - H$. Profiles are generated assuming $\lambda = 6.28\ mm$, a root mean square roughness of the profile $r_{rms} = \left\langle r^2\right\rangle^{1/2} = 1\ \mu m$, $H = 0.7$, and $N = 100$.

Results are averaged on several realizations for each value of h and V, and are shown in terms of the following dimensionless quantities: $\tilde{h} = q_0 h$, $\tilde{a} = q_0 a$, $\tilde{\Delta} = \Delta/\Lambda$, $\tilde{\Lambda} = q_0\Lambda$, $\zeta = q_0 V\tau$, and $\tilde{p} = 2\left(1-\nu^2\right)p/\left(Eq_0\Lambda\right)$.

A. Average contact quantities

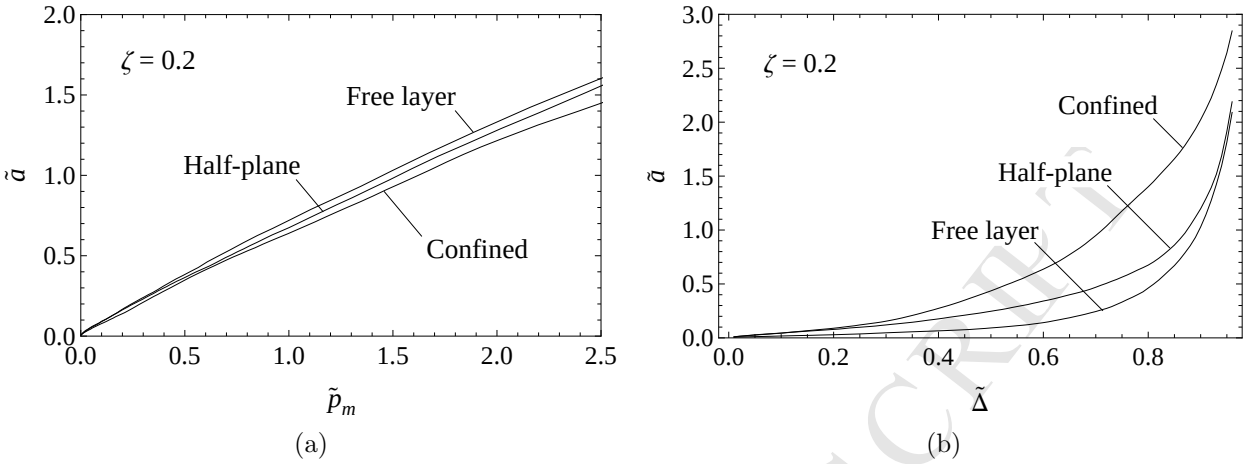

FIG. 2: The dimensionless contact area as a function of contact pressure (a), and contact penetration (b). Results are given for layers with $\tilde{h} = 1$ and for the half-plane case ($h \to \infty$).

Figures 2 show the dimensionless contact area as a function of the dimensionless mean contact pressure (Fig. 2a) and contact penetration (Fig. 2b), at fixed dimensionless velocity $\zeta = 0.2$. Results are given for both the boundary configurations shown in Fig. 1 and for the half-plane case (i.e. thickness $h \to \infty$). Comparing results of Fig. 2, we notice the contact behavior is differently affected by the specific boundary conditions depending on whether load or displacement is controlled.

Indeed, in Fig. 2a, regardless of the boundary constraints, no significant difference is observed between layers and half-plane at sufficiently low contact pressures. To this regard, let us observe that in proximity of a contact spot of length a, the size d of the material region affected by deformation can be roughly estimated as $d \approx a$. Since, at low contact pressures, the contact domain is constituted by multiple contact spots with local size very smaller than the layer thickness, boundary conditions and finite thickness of the system negligibly affect its contact behavior.

On the other hand, increasing the contact pressure, the contact spots get bigger, and $d \approx a$ can become also larger than h. Under these conditions, the contact configuration and the layer thickness play a more important role in the final contact behavior. In particular, for the confined layer, we observe a smaller contact area compared with the half-plane as a result of the rigid constraint applied on the upper boundary, which makes the whole system stiffer. On the contrary, for the free layer, higher contact areas are observed when the average pressure is increased because it is overall more compliant.

However, the presence of roll-off in the roughness PSD would lead to a higher number of contact spots of the same size $d \approx a \ll h$, but closer one to each other. In this case, even at very low contact pressure, elastic interaction between contact spots will lead to a macroscopic deformed region of size $d \gg a$. In this case, it is not enough that the film thickness is much larger than a single contact region, so different results can occur depending on the specific boundary configuration

Of course, for all configurations the dimensionless contact size $\tilde{a}$ tends to π at the complete contact, as more clearly shown in Fig. 2b, where the contact area is plotted in terms of the penetration. In this case, working at fixed penetration, a reverse scenario is observed and the larger contact areas are obtained for the confined layer. This can be easily explained, consistently with Refs. [2, 46], by observing that, due to the material incompressibility and rigid constraint, at given penetration Δ, the volume of the material displaced by the rough profile peaks must be balanced by an equivalent one which partially fills the valleys, thus increasing the contact area (see Fig.3a). Such a mechanism does not take place in the case of free layer (see Fig.3a), whose contact behavior at small Δ is instead mainly governed by bending (as observed in Refs. [2, 46]), resulting in negligible influence of Δ on the contact area. However, at large values of Δ, a small increment in penetration causes a strong increase in contact area as, close to complete contact, most of the peaks are already in contact and further bending deformation is inhibited. Under this condition, local interfacial deformation occurs that is governed by the local contact stiffness, proportional to the ratio a/h, as demonstrated in Ref. [2].

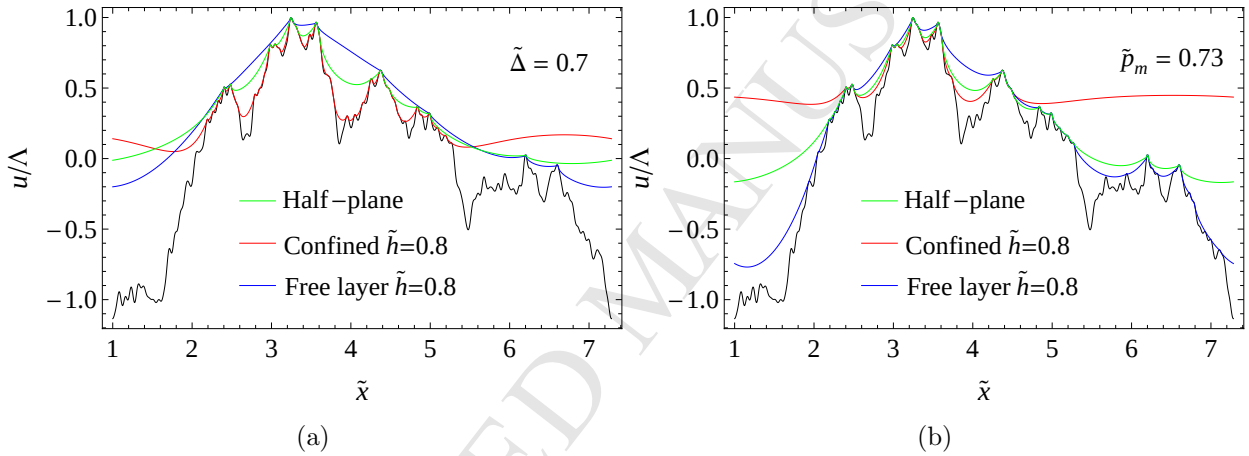

FIG. 3: The deformed profiles of the viscoelastic bodies at given contact penetration (a), and mean contact pressure (b). Results are given for layers with $\tilde{h} = 0.8$ and for the half-plane case ($h \to \infty$).

Similar conclusions can be drawn by Fig. 3, where the deformed profile of the viscoelastic bodies is shown under displacement (Fig.3a) and load (Fig. 3b) controlled conditions. Results are given for the half-plane case, and for the confined and free layer with $\tilde{h} = 0.8$. At given contact penetration (see Fig. 3a), the confined layer shows a much larger number of contact spots and overall contact area compared to the free layer. Vice versa, under load controlled conditions (see Fig. 3b), the behavior reverses with the free layer showing a slightly larger contact area and a larger number of contact spots, due to its lower contact stiffness (see Ref. [2]).

Fig. 4 shows the dependence of the dimensionless contact mean pressure on the dimensionless sliding speed ζ, at fixed penetration $\tilde{\Delta} = 0.35$. For all the contact configurations we observe a monotonic increase of $\tilde{p}_m$ with ζ because of the viscoelastic material response. In fact, increasing ζ, the frequency of excitation ω increases and a progressive transition from the soft rubbery region to the hard glassy one occurs. Notice also the mean pressure values calculated at high and low speeds are almost in the same ratio as the elastic moduli

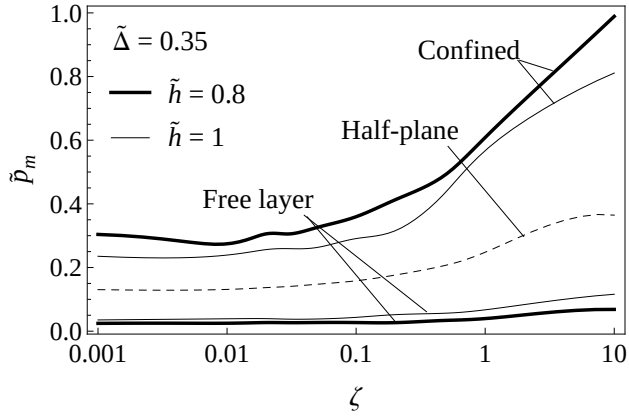

FIG. 4: The dimensionless mean contact pressure as a function of the dimensionless sliding velocity for fixed $\tilde{\Delta} = 0.35$. Results are given for layers with $\tilde{h} = 1$ and for the half-plane case ($h \to \infty$).

$E_\infty/E_0 = 3$. Finally, according to previous results given in Ref. [46], we notice that both the free and confined layer approach the half-plane solution as h is increased.

B. The viscoelastic friction

Viscoelastic materials present bulk viscous dissipation proportional to the first time derivative of the applied strains. This dissipation gives rise to macroscopic reactions, which oppose the strain change. In the specific case of sliding contacts, a macroscopic reaction force is developed contrasting the relative motion between the bodies, which is usually referred to as *viscoelastic* friction. Of course, an asymmetrical contact pressure distribution within each contact spot must occur for this force to develop (see, for example, [46, 54]).

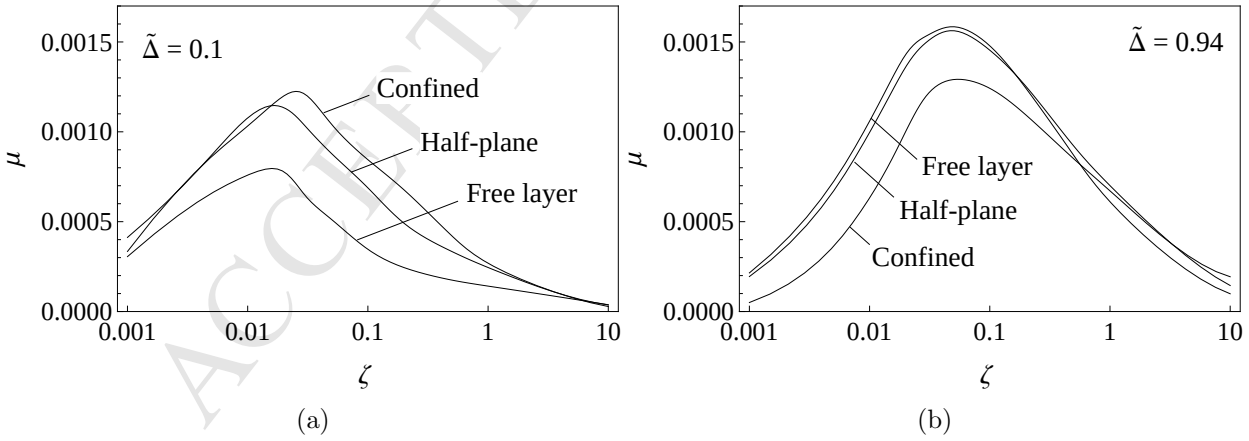

FIG. 5: The viscoelastic friction coefficient μ as a function of the dimensionless sliding velocity ζ for $\tilde{\Delta} = 0.1$ (a), and $\tilde{\Delta} = 0.94$ (b). Results are given for layers with $\tilde{h} = 1$ and for the half-plane case ($h \to \infty$).

Fig. 5 shows the viscoelastic friction coefficient as a function of ζ for fixed low (Fig. 5a)

and high (Fig. 5b) contact penetration. In all cases the curves are characterized by a bell-shaped trend. This can be explained by arguing that the dissipated energy per unit time is related to the imaginary part $\Im[E(\omega)]$ of the viscoelastic modulus, which typically has a bell-shaped dependence on the frequency $\omega \propto V$ of excitation. Therefore, at low and high frequencies (the "rubbery" and "glassy" regions, respectively), the imaginary part $\Im[E(\omega)]$ vanishes, thus leading to vanishing values of the energy dissipation. For this reason, in the limit of small and large velocities the response of the material is practically elastic (with elastic modulus respectively equal to E_0 and E_∞), and the friction coefficient vanishes. At intermediate ranges of velocity (the so called "leathery" or "viscoelastic" region), viscoelastic friction occurs as a result of the viscous dissipation (with a maximum that will be located approximately at a frequency of excitation $\omega \approx 1/\tau$, being τ the relaxation time of the material).

Notice at small contact penetrations (Fig. 5a) higher values of the friction coefficient are observed for the rigidly confined layer. On the contrary, when the penetration is increased (Fig. 5b), the contact involves much more material and the behavior reverses, with the free layer showing almost the same μ of the half-plane, but significantly higher than the confined one.

The above result occurs because, at high Δ, bending involves the whole layer when its upper edge is free. Vice versa, when the layer is constrained on the top, bending is inhibited and smaller regions are involved by the viscoelastic deformation.

At low Δ, the friction coefficients for the two investigated contact configurations are almost in the same ratio as the contact areas (see Ref. [46]). Then a smaller friction coefficient is obtained for the free layer that shows smaller contact areas at fixed penetration (see Fig. 2b).

IV. COMPARISON WITH PERSSON'S THEORY

In this section, according to the procedure defined in Appendix B, we propose a comparison with a 1D version of the Persson's theory [18], where, as suggested by the author in Refs. [18, 19], we assume that the only fitting parameter of the theory takes the value $\beta = 0.48$.

In Fig. 6a we compare the numerically calculated contact area with the theoretical predictions of Persson's theory. In particular, the contact area is shown as a function of the sliding velocity, for a given remote load $\tilde{p}_m = 1.3$. Regardless of the specific configuration (half-space, confined layer or free layer), the contact area decreases with the velocity because increasing the sliding velocity causes the viscoelastic stiffening of the material. The figure shows some differences between our calculations and Persson's theory, however in our opinion the agreement can be considered more than satisfactory, also considering that Persson's theory is a renormalization group approach, which is more accurate in the 2D case.

Interestingly, Fig. 6b shows the PSDs of the numerically calculated deformed profiles compared to those predicted by the Persson's theory. We observe a significant agreement for the half-space (already observed for the elastic substrate in Ref. [57]) and free layer configurations. A certain degree of disagreement is observed for the confined layer case in the range of low wavevectors. This partial disagreement, has to be ascribed to the fact that real or numerically generated rough surfaces are finite and, as such, the tail of the asperity heights distribution is truncated to finite values. This allows the finite rough surface to be totally confined beneath the rigid plate that constrains the displacement on

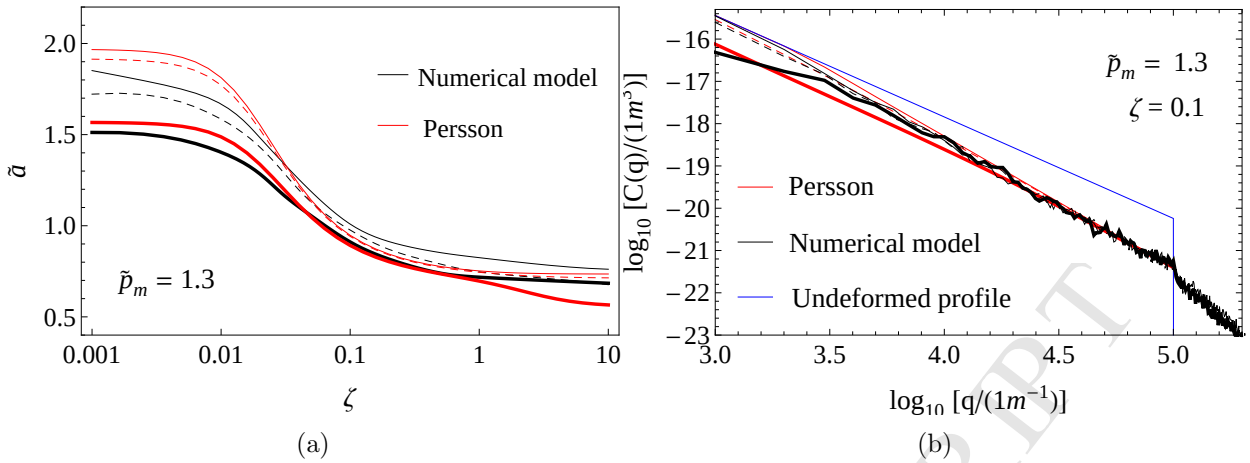

FIG. 6: A comparison between numerical results (in black) and Persson's theory predictions (in red) for: (a) the dimensionless contact area as a function of the dimensioless sliding velocity; (b) the deformed profile PSD. Dashed lines refer to the half-plane case ($h \to \infty$), thick and thin lines to the confined and free layer cases with $\tilde{h} = 1$, respectively.

the upper part of the layer [Fig 1(a)]. In Persson's theory - which is a statistical theory - things are a little different. In fact asperities of any heights, also those whose height exceed the thickness h of the layer, are included in the calculations. Thus, despite the right boundary conditions are still fulfilled thanks to the use of the correct Green's function [see Eq. (5)] interpenetration of the elastic body with the rigid plate can actually occur in the theory, leading to a deviation from the numerical calculation just for wavevectors $q < 2\pi/h$. Of course, this interpenetration does not take place for the half-space and free layers configurations, where indeed the agreement with Persson's theory is very good.

We also note that, due to the intrinsic (geometric) non-linearity of the contact problem, deformation occurring at different wavelengths (i.e. at different $q-$vectors) are not really independent, thus leading, as predicted by our numerical calculations, to non-vanishing PSD for wavevectors $q > q_1$, *i.e.* at spatial frequency at which the spectrum of the rigid rough profile PSD vanishes.

Fig. 7 shows the friction coefficient as a function of the dimensionless sliding velocity ζ, at fixed mean contact pressure $\tilde{p}_m = 1.3$. At small velocities ζ, the Persson's theory predicts a slightly smaller friction coefficient compared to numerical results. Such a trend is reversed as ζ is increased. The observed difference is related to the frictional contribution ascribed to very short length scales (i.e. $q > q_1$) which cannot be taken into account in the Persson's theory (see Fig. 6b). In fact, at low sliding velocities, the cyclic deformations associated with very short length scales will also contribute to the hysteretic dissipation into the material as they will excite the viscoelastic material in a range of frequencies close to the transition region of its viscoelastic spectrum. As a result, the peak value of the coefficient of friction predicted by numerical calculations has to be shifted, when compared with Persson's predictions, towards lower values of the sliding velocity, as indeed is observed in Fig. 7. On the contrary, for sufficiently large ζ, the excitation induced by very short length scales will fall into the glassy region of the viscoelastic spectrum of the material, and will not contribute to the hysteretic dissipation, *i.e.* to friction coefficient, leading to a better agreement with Persson's theory.

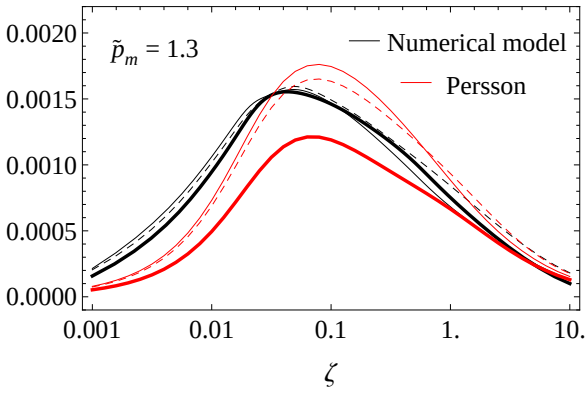

FIG. 7: The dependence of the friction coefficient on the dimensionless sliding velocity at fixed $\tilde{p}_m = 1.3$. Comparison between Persson's theory predictions (in red) and numerical simulations (in black). Dashed lines refer to the half-plane case ($\tilde{h} \to \infty$), whereas thick and thin lines refer to the confined and free layer cases with $\tilde{h} = 1$, respectively.

It is worth noticing that, at fixed load, the geometry of the system does not significantly affect the friction coefficient μ. This is in contrast with results given in Fig. 5 where the friction coefficient is calculated at fixed penetration. A possible explanation of such a behavior relies on the observation that the amount of dissipated energy strongly depends on the amount of material involved in the cyclic deformation caused by each single asperity. This volume of material can be roughly assumed proportional to the square of each asperity contact size. So now, if we look at the contact area, when the controlled quantity is the remote load $\tilde{p}_m$, curves in Fig. 2(a) show that differences between the free layer, the confined layer and the half-space are much less significant if compared to those observed when the controlled parameter is the penetration $\tilde{\Delta}$ [see Fig. 2(a)]. This also explains why, in Fig. 5, we observe a more significant dependence of μ on the geometry of the system and boundary conditions.

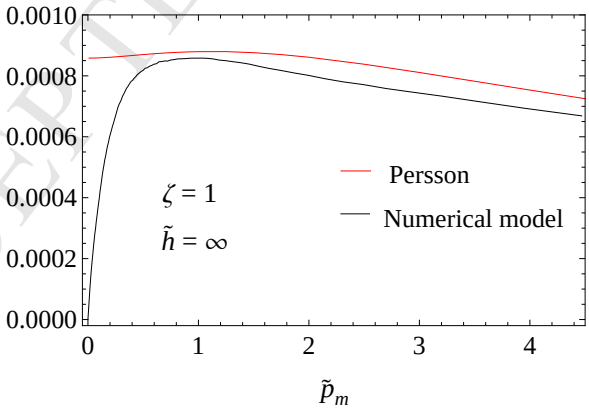

FIG. 8: A comparison between the Persson's theory predictions (in red) and the numerical results (in black) for the friction coefficient as a function of the dimensionless mean contact pressure. Results refers to the half-plane case.

In fig. 8, the friction coefficient is plotted in terms of the mean contact pressure $\tilde{p}_m$, at fixed $\zeta = 1$. For $\tilde{p}_m > 1$ numerical results and Persson's theory predictions run sufficiently

close and almost parallel to each other. At low mean pressure, numerical data show an increasing larger deviation from the Persson's predictions as $\tilde{p}_m$ vanishes because of the finiteness of our numerically generated surfaces.

V. CONCLUSIONS

The sliding contact of a linear viscoelastic layer on a randomly rough rigid profile is investigated. Specifically, three different configurations are taken into account: (a) a layer rigidly constrained on the upper boundary, (b) a free layer uniformly loaded on the top, (c) the half-space case.

Results show that the specific boundary conditions, as well as the layer thickness, strongly affect the contact and frictional behavior of the system, in terms of mean contact area and friction coefficient. In particular, the layer rigidly constrained turns out stiffer than the free layer uniformly loaded. The half-space behavior lies halfway between the two limiting cases Interestingly, we found that depending on the controlled parameter (*i.e.* load or displacement) different results can be achieved in terms of contact behavior. Indeed, under load controlled conditions the free layer shows larger contact area compared to the confined one, whereas the opposite scenario is observed when displacement is controlled. Further, the choice of the controlled parameter also affects the dependence of the system behavior on the boundary conditions. For instance, the friction coefficient at fixed load does not significantly depend on the system configuration, whereas differences are much more remarkable when displacement is controlled.

Finally, we performed a detailed comparison with the predictions of the most advanced version of Persson's theory. Comparison was made in terms of contact and frictional behavior. Specifically, numerical calculations and theoretical predictions show the same 'bell shaped' dependency of the friction coefficient on the sliding velocity, with the peak located in the frequency region where $\Im\left[E\left(\omega\right)\right]$ is close to the maximum. In this respect, a very good quantitative agreement is found for the free layer and half-space cases. However, a certain degree of disagreement due to finite size effects is found for the confined layer case, in the low range of q-vectors.

APPENDIX A: ROUGH PROFILE GENERATION

Here we summarize the procedure already presented in Ref. [58] to numerically generate a rough profile

$$r\left(x\right)=\sum_{k=1}^{N}r_k\cos\left(kq_0x+\phi_k\right) \tag{A1}$$

where N is the number of roughness scales of the profile.

Firstly, we observe that for any self-affine profile $r\left(x\right)$ the statistical properties are invariant under the transformation

$$x\rightarrow tx;\qquad r\rightarrow t^Hh \tag{A2}$$

in such a case it can be shown that the power spectral density (PSD) is

$$C\left(q\right)=\frac{1}{2\pi}\int\left\langle r\left(x'\right)r\left(x'+x\right)\right\rangle e^{-iqx}=C_0\left(\frac{|q|}{q_0}\right)^{-(2H+1)} \tag{A3}$$

where the symbol $\langle\rangle$ stands for the ensemble average linear operator. We observe that, because of translational invariance, the autocorrelation function $\langle r(x')\, r(x'+x)\rangle$ satisfies the relation $\langle r(x')\, r(x'+x)\rangle = \langle r(0)\, r(x)\rangle$. Eq. (A3) shows that only three parameters are needed to fully characterize the PSD of the profile. The amplitudes r_k and the phases ϕ_k of the harmonic terms [see Eq. (A1)] need to be determined in such a way that the resulting profile is Gaussian with the PSD given in Eq. (A3).

First observe that in order to satisfy the translational invariance of the profile statistical properties, it is enough to assume that the random phases ϕ_k are uniformly distributed on the interval $[-\pi, \pi[$. In such a case the autocorrelation function takes the form

$$\langle r(x')\, r(x'+x)\rangle = \sum_{k=1}^{N} \frac{\langle r_k^2\rangle}{2} \cos(kq_0 x) \tag{A4}$$

Now we need to calculate the quantities $\langle r_k^2\rangle$. To this purpose let us calculate the PSD of the periodic profile given in Eq. (A1). By using the definition we get

$$C(q) = \frac{1}{2\pi} \sum_{k=1}^{N} \int dx \frac{\langle r_k^2\rangle}{2} \cos(kq_0 x)\, e^{-iqx} = \sum_{k=1}^{N} \frac{1}{4} \left[\left\langle r_k^2\right\rangle \delta(q - kq_0) + \left\langle r_k^2\right\rangle \delta(q + kq_0)\right] \tag{A5}$$

from which it follows that

$$C(-kq_0) = C(kq_0) = C_k = \frac{\langle r_k^2\rangle}{4} \delta(0) \tag{A6}$$

where $\delta(q)$ is the Dirac delta function. Using Eq. (A3) and observing that $C_0 = \langle r_1^2\rangle \delta(0)/4$, one obtains

$$\left\langle r_k^2\right\rangle = \left\langle r_1^2\right\rangle k^{-(2H+1)} \tag{A7}$$

Hence, the quantities $\langle r_k^2\rangle$ can be determined once known $\langle r_1^2\rangle$ and the Hurst exponent of the surface. Now observe that from Eq. (A4) $\left\langle r(x)^2\right\rangle = \sum_{k=1}^{N} \langle r_k^2\rangle /2$, and using Eq. (A7) yields

$$m_0 = \int C(q) dq = \left\langle r(x)^2\right\rangle = \frac{\langle r_1^2\rangle}{2} \sum_{k=1}^{N} k^{-(2H+1)} \tag{A8}$$

Therefore, if one knows the zero-th order moment m_0 of the power spectral density, i.e. the mean square value of the profile heights $m_0 = r_{\text{rms}}^2 = \left\langle r(x)^2\right\rangle$, one can calculate $\langle r_1^2\rangle$ and therefore all other quantities $\langle r_k^2\rangle$. However to completely characterize the rough profile we still need the probability distribution of the amplitudes r_k. There are several choices, however the simplest assumption, as suggested by Persson et al. in Ref. [59], is that the probability density function of r_k is just a Dirac delta function centered at $[4C_k/\delta(0)]^{1/2} \approx 2(q_0 C_k)^{1/2}$

$$p(r_k) = \delta\left(r_k - 2\sqrt{q_0 C_k}\right) \tag{A9}$$

i.e. we assume that $r_k = 2\sqrt{q_0 C_k}$. In the above relations we have used that $\delta(q=0) \approx q_0^{-1} = \lambda/(2\pi)$. It can be shown [59] that Eq. (A9) also guarantees that the random profile $r(x)$ is Gaussian.

The three parameter employed to characterize the statistical properties of the surface are the Hurst exponent H, the zero-th order moment of the roughness PSD

$$m_0 = \left\langle r^2(x) \right\rangle = 2q_0 C_0 \sum_{k=1}^{N} k^{-1-2H} \tag{A10}$$

and the second moment of the PSD

$$m_2 = \left\langle r'^2(x) \right\rangle = \left\langle (\nabla r)_{1D}^2 \right\rangle = \int q^2 C(q) dq = 2q_0^3 C_0 \sum_{k=1}^{N} k^{1-2H} \tag{A11}$$

Interestingly, we observe that since $0 < H < 1$ the sum $\sum_{k=1}^{N} k^{1-2H}$ does not converge as N is increased, i.e. as more and more spectral components are included in the rough profile. However, we also observe that, when $H > 0.5$, the slope $q_k r_k = 2\sqrt{q_0^3 C_0} k^{(1-2H)/2}$ of each single Fourier component of the rough profile decreases as k is increased, with a faster decrease for higher values of H. Since real surfaces most of times present Hurst exponent larger than 0.7, we may say that for real surfaces the shortest wavelengths components of the roughness are smoother than long wavelength components.

APPENDIX B: THE 1D VERSION OF THE PERSSON'S THEORY

In this appendix we present an extension of the Persson's theory [18] to the case of 1D line contacts. In Ref. [37], moving from the original Persson's theory [17], the expression of the coefficient of friction for steady sliding (along the x-axis) at velocity V against a 2D surface with anisotropic statistical properties has already been developed (see Eqs. (20-22) in Ref. [37]). Here, coherently with the further corrections to the Persson's theory presented in [18, 19] for the case of elastic contacts, we introduce the correcting factor $T(q) = \beta + (1-\beta)P^2(q)$ also in the case of viscoelastic contacts. Therefore, moving from Eqs. (20-22) in Ref. [37], we have

$$\mu = \frac{1}{2} \int_{-\infty}^{\infty} d^2q \; q q_x C_{2D}(\mathbf{q}) T(q) P(q) \operatorname{Im} \left[\frac{E(q_x V)}{(1-\nu^2) S(qh) p_m} \right] \tag{B1}$$

where $q = |\mathbf{q}|$, and $\mathbf{q} = (q_x, q_y)$. Notably, $S(qh) = S(mq_0 h) = -A_m(q_0 h) + 1$, where A_m depends on the specific boundary condition, as given by Eqs. (5-7).

$$P(q) = \frac{A(q)}{A_0} = \operatorname{erf}\left(\frac{1}{2\sqrt{G(q)}} \right) \tag{B2}$$

is the apparent area of contact at the magnification q/q_0. Further, we have that

$$G(q) = \frac{1}{8} \int_{-\infty}^{\infty} d^2q \; q^2 C_{2D}(\mathbf{q}) T(q) \left| \frac{E(q_x V)}{(1-\nu^2) S(qh) p_m} \right|^2 \tag{B3}$$

Now, we recall that, a 1D rough profile can be generalized to an equivalent 2D surface by requiring that the roughness does not change along one of the axis. Therefore, assuming

to have roughness only along the x-axis, following [37], we have that $C_{2D}(\mathbf{q}) = C(q_x)\,\delta(q_y)$, where $C(q_x)$ is the PSD of the 1D rough profile. Substituting in Eq. (B1) we find

$$\mu = \int_0^\infty dq_x \;\; |q_x|\, q_x C(q_x)\, T(q_x)\, P(|q_x|)\, \mathrm{Im}\left[\frac{E(q_x V)}{(1-\nu^2)\, S(qh)\, p_m}\right] \tag{B4}$$

Similarly, from Eq. (B3), we have that

$$G(q) = \frac{1}{4}\int_0^\infty dq_x \; q_x^2 C(q_x)\, T(q_x) \left|\frac{E(q_x V)}{(1-\nu^2)\, S(qh)\, p_m}\right|^2 \tag{B5}$$

[1] Carbone, G., Scaraggi, M., and Tartaglino, U., Adhesive contact of rough surfaces: Comparison between numerical calculations and analytical theories, Eur. Phys. J. E, 2009;30:65–74, .

[2] Menga, N., L. Afferrante, and G. Carbone. Adhesive and adhesiveless contact mechanics of elastic layers on slightly wavy rigid substrates. International Journal of Solids and Structures 2016;88:101-109.

[3] Menga, N., Carbone, G., & Dini, D. Do uniform tangential interfacial stresses enhance adhesion? Journal of the Mechanics and Physics of Solids 2018;112:145-156.

[4] Theodore, A. N., Samus, M. A., & Killgoar Jr, P. C. Environmentally durable elastomer materials for windshield wiper blades. Industrial & engineering chemistry research 2017;31(12): 2759-2764.

[5] Dimaki, A. V., Dmitriev, A. I., Menga, N., Papangelo, A., Ciavarella, M., Popov, V. L. Fast High-Resolution Simulation of the Gross Slip Wear of Axially Symmetric Contacts. Tribology Transactions 2016;59:189-194.

[6] Menga, Nicola, and Michele Ciavarella. "A Winkler solution for the axisymmetric Hertzian contact problem with wear and finite element method comparison." The Journal of Strain Analysis for Engineering Design 2015;50.3:156-162.

[7] Pereira, K., Yue, T., & Wahab, M. A. Multiscale analysis of the effect of roughness on fretting wear. Tribology International2017;110:222-231.

[8] Bottiglione, F., Carbone, G., & Mantriota, G. Fluid leakage in seals: An approach based on percolation theory. Tribology international 2009;42(5):731-737.

[9] Dapp, W. B., Lücke, A., Persson, B. N., & Müser, M. H. Self-affine elastic contacts: percolation and leakage. Physical review letters 2012;108(24):244301.

[10] Afferrante, L., & Ciavarella, M. The thermoelastic Aldo contact model with frictional heating. Journal of the Mechanics and Physics of Solids 2004;52(3):617-640.

[11] Afferrante, L., & Ciavarella, M. Instability of thermoelastic contact for two half-planes sliding out-of-plane with contact resistance and frictional heating. Journal of the Mechanics and Physics of Solids 2004;52(7):1527-1547.

[12] Yi, F., Zhang, M., & Xu, Y. Effect of the electric current on the friction and wear properties of the CNT–Ag–G composites. Carbon 2015;43(13):2685-2692.

[13] Archard, J.F., Elastic Deformation and the Laws of Friction, Proceedings of the Royal Society of London. Series A 1957;243(1233):190-205.

[14] Greenwood, J.A. and Williamson, J.B.P., Contact of nominally flat surfaces, Proc. R. Soc. Lond. A 1966;295:300–319.

[15] Bush, A.W., Gibson, R.D., Thomas, T.R., TheElastic Contact of a Rough Surface, Wear 1975;35:87-111.

[16] Afferrante L., Carbone G. and Demelio G., Interacting and coalescing Hertzian asperities: a new multiasperity contact model. Wear 2012;278-279:28-33.

[17] Persson B.N.J.,Theory of rubber friction and contact mechanics, Journal of Chemical Physics 2001;115:3840 -3861.

[18] B.N.J. Persson, On the elastic energy and stress correlation in the contact between elastic solids with randomly rough surfaces, J. Phys.: Condens. Matter 2008;20(31).

[19] Yang, C. and Persson, B.N.J., Molecular Dynamics Study of Contact Mechanics: Contact Area and Interfacial Separation from Small to Full Contact, Phis, Rev. Lett. 2008;100.

[20] A. Almqvist, C. Campana, N. Prodanov, B.N.J. Persson, Interfacial separation between elastic solids with randomly rough surfaces: comparison between theory and numerical techniques, J. Mech. Phys. Solids 2011;59:2355–2369.

[21] Hunter S.C. , The rolling contact of a rigid cylinder with a viscoelastic half space Trans. ASME, Ser. E, J. Appl. Mech. 1961;28:611–617.

[22] Grosch K. A. , The Relation between the Friction and Visco-Elastic Properties of Rubber, Proceedings of the Royal Society of London. Series A 1963;274(1356):21-39.

[23] Borri-Brunetto, M., Chiaia, B., Ciavarella, M., Incipient sliding of rough surfaces in contact: a multiscale numerical analysis, Comput. Meth. Appl. Mech. Eng. 2001;190:6053-6073.

[24] Hyun, S., Pei, L., Molinari, J.-F., Robbins, M.O., Finite-element analysis of contact between elastic self-affine surfaces, Phys. Rev. E 2004;70.

[25] Campana C., Mueser M.H. and Robbins M.O., Elastic contact between self-affine surfaces: comparison of numerical stress and contact correlation functions with analytic predictions. J. Phys. Condens. Matter 2008;20(35).

[26] Pastewka, L., & Robbins, M. O. Contact area of rough spheres: Large scale simulations and simple scaling laws. Applied Physics Letters 2016;108(22):221601.

[27] Carbone G. and Putignano C., A novel methodology to predict sliding and rolling friction of viscoelastic materials, Theory and experiments, J. of Mech. and Phys. Solids 2013;61:1822-1834.

[28] Medina S. and Dini D., A numerical model for the deterministic analysis of adhesive rough contacts down to the nano-scale. International Journal of Solids and Structures 2014;51(14):2620-2632.

[29] Ilincic, S., Vorlaufer, G., Fotiu, P. A., Vernes, A., & Franek, F. Combined finite element-boundary element method modelling of elastic multi-asperity contacts. Proceedings of the Institution of Mechanical Engineers, Part J: Journal of Engineering Tribology 2009;223(5):767-776.

[30] L. Nasdala, M. Kaliske, A. Becker, H. Rothert, An efficient viscoelastic formulation for steady-state rolling structures, Computational Mechanics 1998;22:395-403.

[31] Le Tallec P., Rahler C., Numerical models of steady rolling for non-linear viscoelastic structures in finite deformations, International Journal for Numerical Methods in Engineering 1994;37:1159-1186.

[32] Afferrante L. Ciavarella M. and Demelio G., Adhesive contact of the Weierstrass profile, Proc. R. Soc. A 2015;471. Doi: 10.1098/rspa.2015.0248.

[33] Solhjoo, S., & Vakis, A. I. Continuum mechanics at the atomic scale: Insights into non-adhesive contacts using molecular dynamics simulations. Journal of Applied Physics 2016;120(21).

[34] Schapery R.A., On the characterization of nonlinear viscoelastic materials, Polymer Engineer-

ing & Science 1969;9(4):295-310.

[35] Faisca R.G, Magluta C. and Roitman N., Experimental Characterization of Viscoelastic Materials as Vibration Dampers, Journal of Engineering Mechanics 2001;127(9):959-962.

[36] Odegard G.M., Gates T.S. and Herring H.M., Characterization of viscoelastic properties of polymeric materials through nanoindentation, Experimental Mechanics 2005;45(2):130-136.

[37] Carbone G., Lorenz B., Persson B.N.J. and Wohlers A., Contact mechanics and rubber friction for randomly rough surfaces with anisotropic statistical properties, The European Physiscal Journal E – Soft Matter 2009;29(3):275–284.

[38] Martina D., Creton C., Damman P., Jeusette M. and Lindner A., Adhesion of soft viscoelastic adhesives on periodic rough surfaces, Soft Matter 2012;8(19):5350-5357.

[39] McGhee, A. J., Pitenis, A. A., Bennett, A. I., Harris, K. L., Schulze, K. D., Urueña, J. M., ... & Sawyer, W. G. Contact and Deformation of Randomly Rough Surfaces with Varying Root-Mean-Square Gradient. Tribology Letters 2017;65(4):157.

[40] Batra S.K. and Ling F.F., On deformation friction and interface shear stress in viscoelastic elastic layered system under a moving load, Am. Sot. Lubr. Eng. Trans.1967;10:294-301.

[41] Naghieh G.R., Jin Z.M. and Rahnejat H., Contact characteristics of viscoelastic bonded layers, Applied Mathematical Modelling 1998;22:569-581.

[42] Goryacheva I., Sadeghi F.and Nickel D.A., Internal Stresses in Contact of a Rough Body and a Viscoelastic Layered Semi-Infinite Plane, Journal of Tribology 1996;118(1):131-136.

[43] Persson, B. N. J. Contact mechanics for layered materials with randomly rough surfaces. Journal of Physics: Condensed Matter 2012;24.9:095008.

[44] Scaraggi, M., & Persson, B. N. J. The effect of finite roughness size and bulk thickness on the prediction of rubber friction and contact mechanics. Proceedings of the Institution of Mechanical Engineers, Part C: Journal of Mechanical Engineering Science 2016;230(9):1398-1409.

[45] Carbone G., Mangialardi L., Analysis of adhesive contact of confined layers by using a Green's function approach, The Journal of the Mechanics and Physics of Solids 2008;56(2):684-706.

[46] Menga, N., Afferrante, L. and Carbone, G., Effect of thickness and boundary conditions on the behavior of viscoelastic layers in sliding contact with wavy profiles, The Journal of the Mechanics and Physics of Solids 2016;95: 517-529.

[47] Menga, N., Foti, D., & Carbone, G. Viscoelastic frictional properties of rubber-layer roller bearings (RLRB) seismic isolators. Meccanica 2017;52(11-12):2807-2817.

[48] Müser, M. H., Dapp, W. B., Bugnicourt, R., Sainsot, P., Lesaffre, N., Lubrecht, T. A., ... & Rohde, S. Meeting the contact-mechanics challenge. Tribology Letters 2017;65(4):118.

[49] Putignano C., Dini D. and Carbone G., Mechanics of Rough Contacts in Elastic and Viscoelastic Thin Layers, International Journal of Solids and Structures 2015;60-70:507-517.

[50] Bugnicourt, R., Sainsot, P., Lesaffre, N., & Lubrecht, A. A. Transient frictionless contact of a rough rigid surface on a viscoelastic half-space. Tribology International 2017;113:279-285.

[51] Scaraggi, M., & Persson, B. N. J. Friction and universal contact area law for randomly rough viscoelastic contacts. Journal of Physics: Condensed Matter 2015;27(10):105102.

[52] Scaraggi, M., & Persson, B. N. General contact mechanics theory for randomly rough surfaces with application to rubber friction. The Journal of chemical physics 2015;143(22):224111.

[53] Joe, J., Scaraggi, M., & Barber, J. R. Effect of fine-scale roughness on the tractions between contacting bodies. Tribology International 2017;111:52-56.

[54] Menga N, Putignano C, Carbone G, Demelio GP., The sliding contact of a rigid wavy surface with a viscoelastic half-space. Proc. R. Soc. A 2014;470.

ACCEPTED MANUSCRIPT

[55] Carbone G., Mangialardi L., Adhesion and friction of an elastic half-space in contact with a slightly wavy rigid surface, Journal of the Mechanics and Physics of Solids 2004;52(6):1267-1287.

[56] Maugis, D., Contact Adhesion and Rupture of Elastic Solids. Springer-Verlag Berlin Heidelberg, 2000.

[57] Carbone G., Pierro E., The influence of the fractal dimension of rough surfaces on the adhesion of elastic materials, Journal of Adhesion Science and Technology 2012;26(22):2555-2570.

[58] Bottiglione, F., & Carbone, G. Role of statistical properties of randomly rough surfaces in controlling superhydrophobicity. Langmuir 2012;29(2):599-609.

[59] Persson, B. N. J., Albohr, O., Tartaglino, U., Volokitin, A. I., & Tosatti, E. On the nature of surface roughness with application to contact mechanics, sealing, rubber friction and adhesion. Journal of Physics: Condensed Matter 2004;17(1):R1-R65.

ACCEPTED MANUSCRIPT

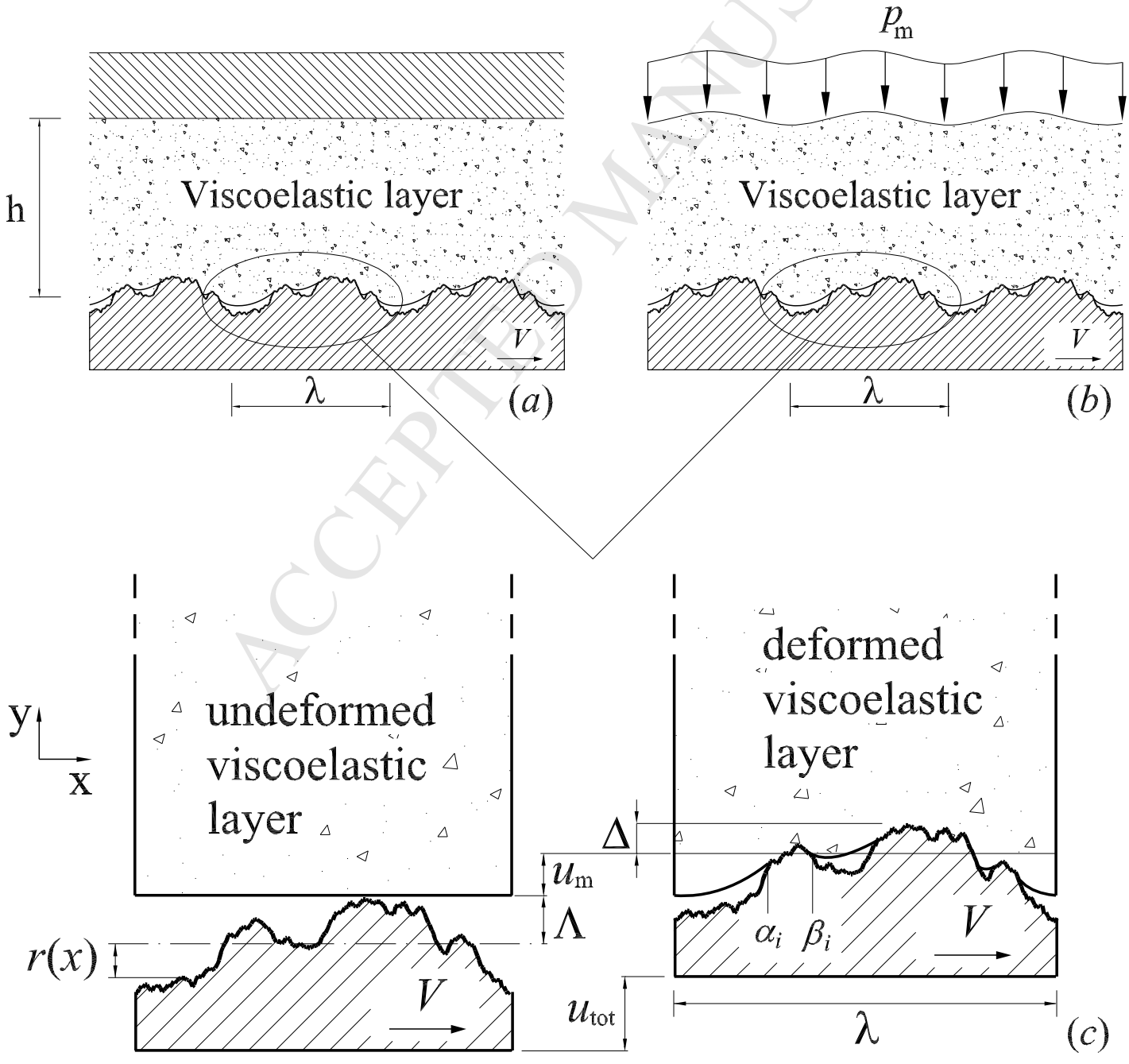

ACCEPTED MANUSCRIPT

ACCEPTED MANUSCRIPT

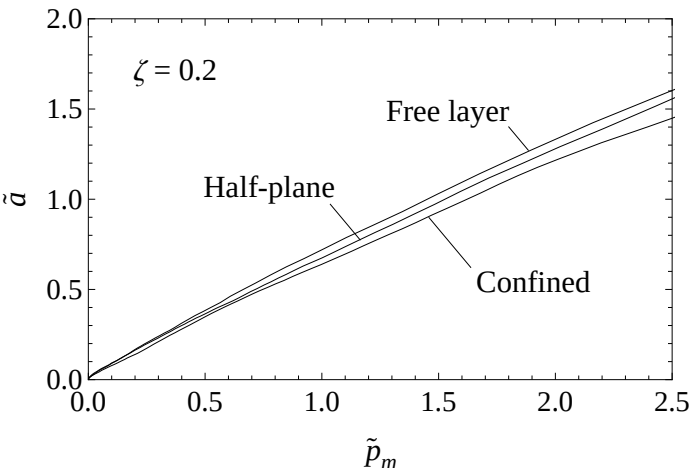

ACCEPTED MANUSCRIPT

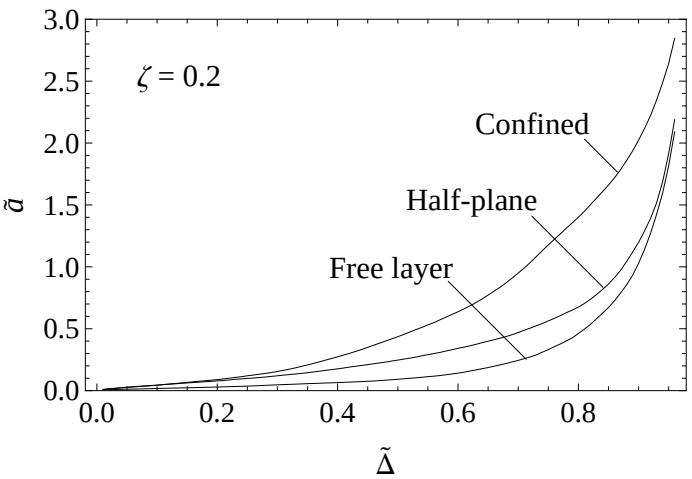

ACCEPTED MANUSCRIPT

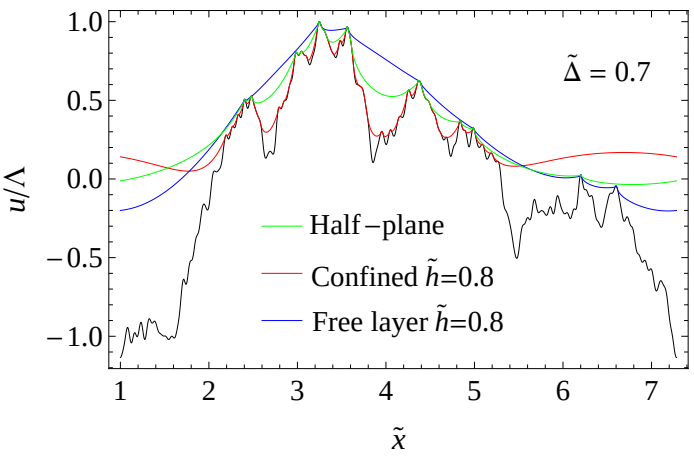

ACCEPTED MANUSCRIPT

ACCEPTED MANUSCRIPT

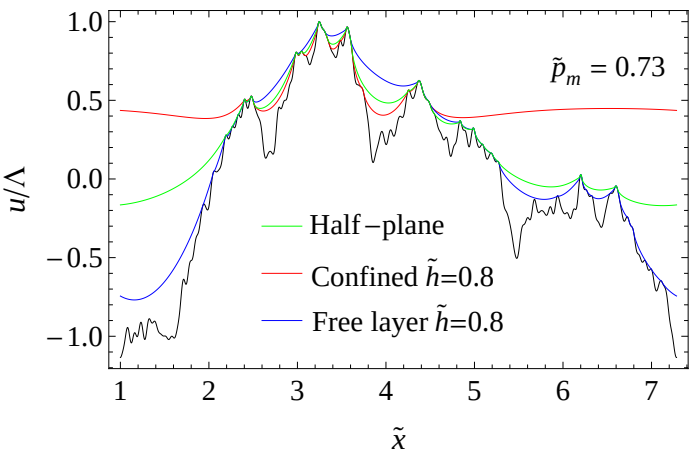

ACCEPTED MANUSCRIPT

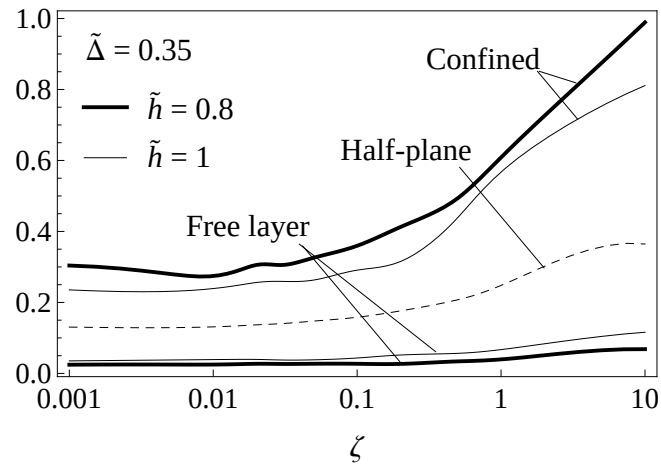

ACCEPTED MANUSCRIPT

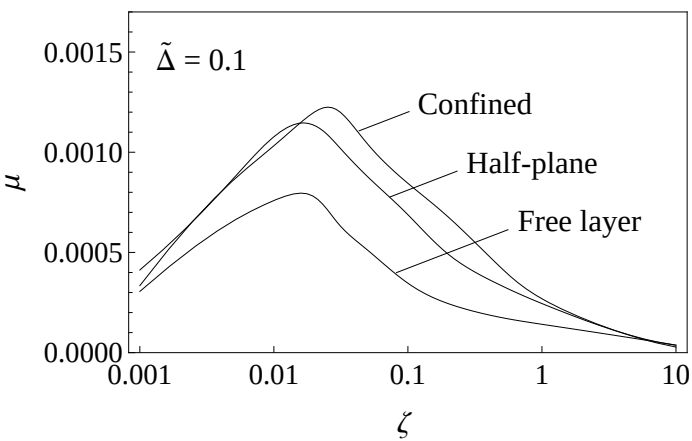

ACCEPTED MANUSCRIPT

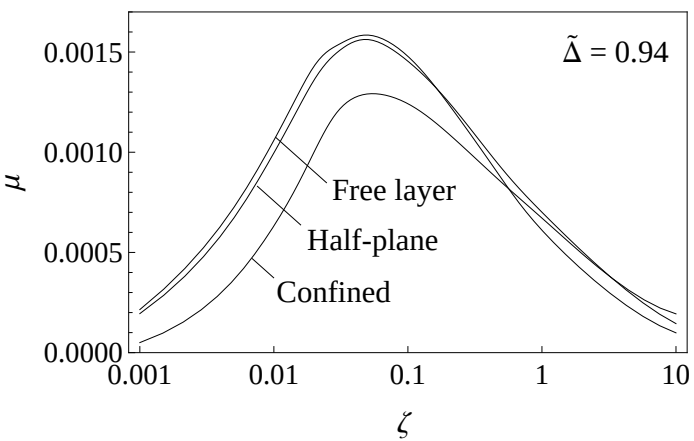

ACCEPTED MANUSCRIPT

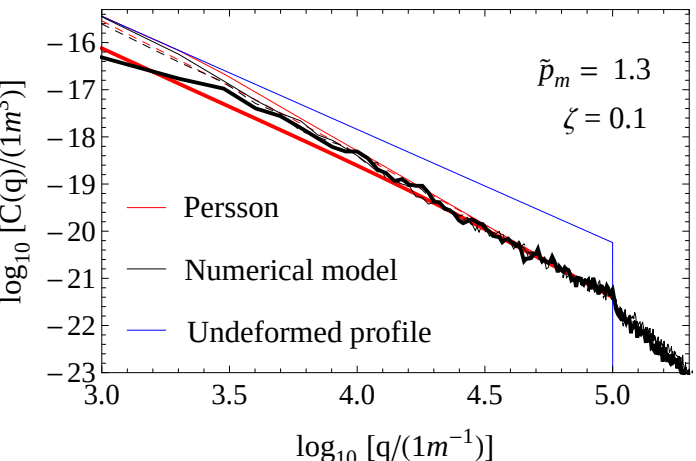

ACCEPTED MANUSCRIPT

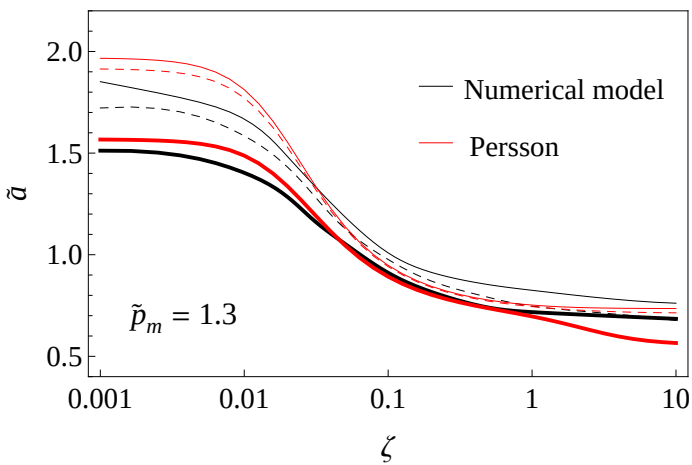

ACCEPTED MANUSCRIPT

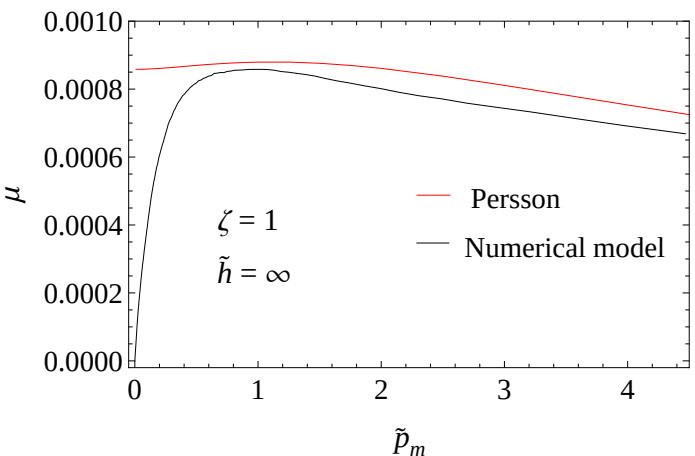

ACCEPTED MANUSCRIPT

ACCEPTED MANUSCRIPT

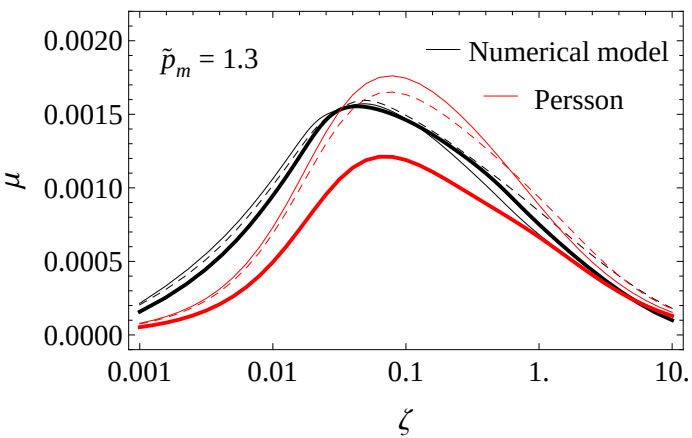

ACCEPTED MANUSCRIPT

- Boundary conditions effects on viscoelastic layer in sliding contact is investigated
- Under load controlled conditions friction is not affected by boundary conditions
- Persson's theory predictions are in good agreement with the numerical calculations

ACCEPTED MANUSCRIPT